Conformational Flexibility of a Ubiquitin Conjugation Enzyme (E2)†

Qin Liu,‡,§ Yate-Ching Yuan,§ Binghui Shen,|| David J. Chen,*,‡ and Yuan Chen*,§

DNA Damage and Repair Group, Life Science Division, Los Alamos National Laboratories, Los Alamos, New Mexico 87545, and Division of Immunology and Department of Cell and Tumor Biology, Beckman Research Institute of the City of Hope, 1450 East Duarte Road, Duarte, California 91010

Received July 31, 1998; Revised Manuscript Received November 30, 1998

ABSTRACT: Ubiquitination plays important roles in a variety of biological processes, such as DNA repair, cell cycle regulation, and p53-dependent processes. Despite intensive studies in ubiquitination, the mechanism of substrate recognition is still not well understood. Each E2 has its own substrate specificity, yet substrate proteins recognized by each E2 are highly diverse. To better understand how E2 proteins confer both substrate specificity and diversity, we have studied conformational flexibility of an E2, UBC9, using nuclear magnetic resonance ^{15}N relaxation and hydrogen−deuterium exchange measurements. Two regions in human UBC9 show higher mobility over a wide range of time scales. Combined with previous biochemical studies, both regions are likely to be important for protein−protein recognition in the ubiquitin pathway. The region near the N-terminus may be important for interactions with the E1-UBL1 conjugate. The region near the C-terminus, which undergoes conformational exchange may be important for substrate binding and catalytic activity. Since E2 enzymes share high homology in primary sequences and three-dimensional structures, the conformational flexibility of UBC9 may represent a general feature of E2 enzymes. This study *provides* a new perspective for further studies of protein−protein recognition in ubiquitination.

Extensive studies have been conducted on ubiquitination (for reviews, see refs *1*−*3*). Ubiquitin, a protein with 76 amino acids, is highly conserved throughout many species. Its C-terminal Gly residue is involved in a covalent conjugation to a Lys residue of other proteins. The C-terminal Gly residue of one ubiquitin molecule may also conjugate to the Lys^{48} of another ubiquitin molecule in multi-ubiquitination. In the ubiquitination pathway, the ubiquitin activation enzyme E1 activates ubiquitin by hydrolyzing ATP to form a high-energy bond with ubiquitin. Ubiquitin is then transferred to a ubiquitin conjugation enzyme (UBC)[1], also known as E2. In this step, the C-terminal Gly is conjugated to the SH group of the active site Cys residue. Interactions between E2 and substrate proteins result in transferring ubiquitin to the substrate proteins. In some cases, this process requires the participation of ubiquitin−protein ligase (E3).

Ubiquitination plays important roles in a variety of biological processes. Ubiquitination mainly participates in protein degradation. Many crucial proteins are degraded by the ubiquitination pathway. These include some cyclins, cyclin-dependent kinase inhibitors, histones, oncogenes, and short-lived transcription factors (*4*−*6*). Ubiquitination has been shown to play key roles in cell cycle control and apoptosis (*7*). Some processes that do not appear to be involved in protein degradation also require ubiquitin. Ubiquitin may serve as a chaperone that targets proteins for cell structure formation, such as biogenesis of peroxisomes (*8*) and ribosomes (*9*), and for protein translocation (*10*). Ubiquitination is highly specific in two aspects. The choice of proteins to be ubiquitinated is highly selective, and the timing of when to ubiquitinate a selected protein, especially in cell cycle control, is highly selective.

Proteins with high sequence homology to ubiquitin, E1, and E2 enzymes have been found. The ubiquitin homologous proteins include the yeast protein SMT3, human protein UBL-1 (also known as SUMO-1, GMP1, PIC1, or sentrin) (for a review, see ref *11*), ISG15 (*12*), and NEDD-8 identified in mice and plants (*13*, *14*). A unique feature of ubiquitin and ubiquitin-like protein is that they all contain a diglycine sequence at the C-terminus which is capable of conjugating to other proteins in the ubiquitin pathway. In addition to ubiquitin homologues, an E1 homologue has also been found (*15*). Many E2 proteins have been found with different substrate specificities. UBC1, UBC4, and UBC5 appear to be involved in general ubiquitination pathways that lead to the degradation of abnormal proteins (*16*, *17*). UBC2 (RAD6) is involved in DNA damage repair and sporulation (*9*). UBC3 (cdc34) participates in the stability control of cyclins (*9*). UBC6 is required for protein translocation through the membrane (*10*). UBC10 is involved in peroxisome biogenesis (*8*). Among the conserved residues in the UBC family of proteins, the fragment containing the ubiquitin accepting Cys residue is highly conserved.

* To whom correspondence should be addressed.

† This work is supported in part by NIH GM54190 (Y.C.). Y.C. is a recipient of the American Cancer Society Junior Faculty Research Award (JFRA-646).

‡ Los Alamos National Laboratories.

§ Division of Immunology, Beckman Research Institute of the City of Hope.

|| Department of Cell and Tumor Biology, Beckman Research Institute of the City of Hope.

[1] Abbreviations: NMR, nuclear magnetic resonance; NOE, nuclear Overhauser effect; UBC, ubiquitin conjugation enzyme, also known as E2.

10.1021/bi981840h CCC: $18.00
Published on Web 01/15/1999

UBC9 is a member of the E2 protein family. Instead of ubiquitin, it conjugates with the ubiquitin homologue, UBL1, in humans. The interaction between UBC9 and UBL1 is specific, since UBC9 does not interact well with ubiquitin and UBL1 does not interact with UBC2 (*18*). UBC9 in yeast, mouse, and human has been identified (*4*, *19*, *18*). It plays critical roles in DNA repair, cell cycle regulation, and p53-dependent processes (*4*). Many proteins which interact with UBC9 have been identified. The human UBC9 has been shown to interact with several important proteins, such as RAD51, RAD52, P53, c-jun, glucocorticoid receptor, the negative regulatory domain of the Wilms' tumor gene product, and human papillomavirus type 16 E1 replication protein (*20*−*22*). Seufert and his colleagues have shown that yeast UBC9 may interact with CLB2, an M-phase cyclin, and CLB5, an S-phase cyclin. Hateboer et al. (*23*) showed that murine UBC9, which has an amino acid sequence identical to that of the human UBC9, binds to the CR2 of adenovirus E1A protein.

The three-dimensional structures of several UBC proteins including the plant *Arabidopsis thaliana* UBC1, yeast UBC4, yeast UBC7, and human/murine UBC9 have been determined by X-ray crystallography (*24*−*27*). These UBC proteins have highly conserved tertiary structures with an RMSD of C^{α} atoms less than 2 Å, excluding two surface loops. The two surface loops occur around amino acid residues 35 and 100 and vary significantly in primary sequences and three-dimensional structures among the four different UBC proteins. The largest variation in sequence and length among different E2 proteins occurs at the loop around residue 100.

Despite the intensive studies in ubiquitination, the mechanism of protein−protein recognition in ubiquitination is still not well understood. Substrate binding sites on E2 are still controversial. The sequence and structural variations of the two surface loops around residues 35 and 100 have been proposed to be responsible for substrate-specific recognitions of different UBC proteins. However, biochemical studies show that the N-terminus, which is close to the two loops in the three-dimensional structure of E2, is important in binding the ubiquitin−E1 conjugate (*28*). In addition, although each E2 protein has specificity for substrate proteins, the proteins recognized by each E2 are highly diverse. An apparent paradox is how E2 proteins confer both substrate specificity and diversity. *The substrate diversity may correlate with the conformational flexibility of E2 molecules.* Thus, a flexible region on an E2 enzyme may possibly be the substrate binding site. In addition, conformational flexibility may be important to the catalytic activity of transferring ubiquitin to substrate proteins. To date, the internal mobility of E2 proteins has not been characterized.

NMR methods have played important roles in characterizing the internal mobilities of proteins. Such methods can provide quantitative information on the dynamic processes of proteins over a wide range of time scales. Heteronuclear relaxation measurements provide information related to protein internal motions on the picosecond to nanosecond time scales (for a review, see ref *29*). Chemical exchange data gives insight into protein dynamics in the microsecond to second time scales. Amide ^1H-^2H exchange experiments provide information on the stability of hydrogen-bonded secondary structures, and allow characterization of dynamic processes on the time scale of minutes to hundreds of hours (*30*). This paper describes the characterization of conformational flexibility of human UBC9 using heteronuclear relaxation and amide $^1H/^2H$ exchange studies. The residues that show higher conformational flexibility are not randomly distributed, but localized in two regions. Combined with previous biochemical studies, these two regions may constitute the binding sites for substrates and the E1−UBL1 conjugates.

MATERIALS AND METHODS

Sample Preparation. Human UBC9 was subcloned into vector PET28 (from Novagen, Inc.). The modified plasmid has an open reading frame that encodes the sequence Met-Gly-$(His)_6$, followed by the sequence of UBC9. *Escherichia coli* containing the expression plasmid were grown at 37 °C in M-9 minimal media supplemented with trace minerals and Basal Medium Eagle vitamins (Gibco). $(^{15}NH_4)_2SO_4$ (1.5 g/L) was used as the nitrogen source. Bacterial cultures were fermented in shaking flasks at 37 °C. Expression of the protein was induced by addition of isopropyl β-D-thiogalactopyranoside (IPTG) to a concentration of 1.0 mM when the culture reached $OD_{595\ nm} = 0.6-0.8$. Then shaking was continued for 3−4 h. The culture was centrifuged, and the bacterial pellets were resuspended in Buffer A (5 mM imidazole, 500 mM NaCl, 20 mM TrisHCl, pH 7.9, and 10 mM DTT). The protein was extracted by sonication and centrifugation at 5000*g* for 15 min. The UBC9 protein was recovered in the supernatant.

The protein was purified on a Ni−NTA column (Qiagen). The supernatant was applied to a Ni−NTA column equilibrated with buffer A. The column was washed with 10 volumes of buffer A, followed by 10 volumes of buffer B (20 mM imidazole, 500 mM NaCl, 20 mM TrisHCl, pH 7.9, and 10 mM DTT), then 6 volumes of buffer C (600 mM imidazole, 500 mM NaCl, 20 mM TrisHCl, pH 7.9, and 10 mM DTT). Approximately 30 mg of protein was purified from one liter of the M-9 culture. NMR experiments were conducted using samples containing 0.3 mM and 0.7 mM UBC9 in 100 mM sodium phosphate, at pH 6.0, and 20 mM DTT in $90\%H_2O/10\%D_2O$.

^{15}N Relaxation Experiments. All ^{15}N relaxation experiments were carried out at 30 °C on a Varian Unity-plus 500 NMR spectrometer equipped with four channels, pulse-shaping and pulse-field-gradient capabilities. Backbone resonances of UBC9 were assigned as described (31). ^{15}N relaxation measurements were carried out using the published methods (32). ^{15}N T_1^{-1} relaxation rates were measured with 6 relaxation delays: 6, 355, 710, 1066, 1421, 1665 ms. These relaxation delays should provide sufficient sampling points as has been shown previously (33). ^{15}N T_2^{-1} experiments were performed with 10 relaxation delays: 17, 33, 50, 67, 84, 100, 134, 150, 167, 184 ms. The delay between pulses in the CPMG sequence was 0.9 ms. A recycle delay of 1.5 s was used for measurement of T_1^{-1} and T_2^{-1} relaxation rates. The spectra measuring ^1H-^{15}N NOE were acquired with a 2 s relaxation delay followed by a 3 s period of proton saturation. The spectra recorded in the absence of proton saturation employed a relaxation delay of 5 s. Each 2D data set consists of 2048 complex points in t_2 and 320 points in t_1 with a spectral width of 11250 H_z in the ^1H dimension and 1241 H_z in the indirectly detected ^{15}N dimension. For

error estimation, duplicated spectra were recorded for NOE, at 355 ms relaxation delay for T_1, and at relaxation delays of 50 and 100 ms for T_2 measurements.

All spectra were processed using FELIX 97.0 software from Molecular Simulations Inc. on a SGI Indigo II workstation. A 90° phase-shifted sine-bell window function followed by a Lorentzian-to-Gaussian transformation was applied to the FID before the Fourier transform. The values of T_1^{-1}, T_2^{-1}, and NOE and the uncertainties were calculated using the relaxation module of FELIX 97.0. Briefly, intensities of resonance peaks in two-dimensional spectra were measured as peak heights. Uncertainties in peak height measurements were determined from duplicated spectra. T_1 and T_2 data were fitted to three- and two-parameter exponential equations using a nonlinear least-squares fitting algorithm. The $\{^1H\}$-^{15}N heteronuclear NOE values were calculated as ratios of peak heights in the spectra recorded with and without ^1H saturation. The average values of NOEs and standard errors were determined from the two data sets.

Analysis of Relaxation Data and Reduced Spectral Density Mapping. The ^{15}N T_1^{-1} and T_2^{-1} relaxation rates and the ^1H-^{15}N NOE are dominated by the dipolar interaction of an ^{15}N nucleus with its attached proton and by chemical shift anisotropy, and are related to spectral density functions as follows (*34*):

$$R_1 = d^2[J(\omega_H - \omega_N) + 3J(\omega_N) + 6J(\omega_H + \omega_N)] + c^2J(\omega_N)$$

$$R_2 = 0.5d^2[4J(0) + J(\omega_H - \omega_N) + 3J(\omega_N) + 6J(\omega_H) + 6J(\omega_H + \omega_N)] + (1/6)c^2[3J(\omega_N) + 4J(0)] + R_{ex}$$

$$NOE = 1 + (\gamma_H/\gamma_N)d^2[6J(\omega_H + \omega_N) - J(\omega_H - \omega_N)]$$

in which

$$d^2 = 0.1\gamma_H{}^2\gamma_N{}^2h^2/(4\pi^2)\langle 1/r_{NH}{}^3\rangle^2$$

$$c^2 = (^2/_{15})\,\gamma_N{}^2H_o{}^2\Delta\sigma^2$$

where γ_N and γ_H are the gyromagnetic ratios of the ^1H and ^{15}N nuclei, respectively; ω_H and ω_N are the ^1H and ^{15}N Larmor frequencies; r_{NH} is the internuclear ^1H-^{15}N distance (1.02 Å); H_o is the magnetic field strength; and $\Delta\sigma$ is the difference of the parallel and the perpendicular components of the assumed axially symmetrical ^{15}N chemical shift tensor and is set to −160 ppm. A spectral density function, $J(\omega)$, is the Fourier transform of the autocorrelation function of an NH vector. The R_{ex} is the sum of the effective rate constants for other pseudo-first-order processes that contribute to transverse relaxation. Reduced spectral density functions $J(0)$, $J(\omega_N)$, and $J(\omega_H)$ were calculated as described (*29*).

Model-Free Calculation. The spectral density functions were represented using the extended model-free formalism (*35, 36*)

$$J(\omega) = {}^2/_5\{S^2\tau_m/[1 + (\omega\tau_m)^2] + (S_f{}^2 - S^2)\tau/[1 + (\omega\tau)^2]\}$$

in which $S^2 = S_f{}^2S_s{}^2$ is the generalized order parameter, where $S_f{}^2$ is the order parameter for motions on the picosecond time scale and $S_s{}^2$ is the order parameter for motions on the nanosecond time scale; $\tau^{-1} = \tau_m{}^{-1} + \tau_e{}^{-1}$, where τ_m is the overall rotational correlation time of the molecule and τ_e is the effective internal correlation time of internal motions. Model-free parameters were determined from the T_1^{-1}, T_2^{-1}, and NOE using the Modelfree program (version 3.1) kindly provided by Professor Arthur G. Palmer, III. For each N−H bond vector, five motional models were considered in the analysis and one model was selected by systematically evaluating each model using F-statistical testing as described (*37*). The procedure is summarized as follows. An initial estimation of the overall tumbling correlation time (τ_m) was obtained from the average T_1/T_2 ratio of NH bond vectors which does not appear to have internal motions on the nanosecond time scales or conformational exchange (R_{ex}). Residues were selected on the basis of two criterias, NOE > 0.6 and satisfying the following conditions (*39*):

$$(\langle T_2\rangle - T_{2,n})/\langle T_2\rangle - (\langle T_1\rangle - T_{1,n})/\langle T_1\rangle \leq 1.5\sigma$$

where, $\langle T_1\rangle$ and $\langle T_2\rangle$ are the averages of T_1 and T_2, respectively; $T_{1,n}$ and $T_{2,n}$ are the T_1 and T_2 for residue n, respectively; σ is the standard deviation of $(\langle T_2\rangle - T_{2,n})/\langle T_2\rangle - (\langle T_1\rangle - T_{1,n})/\langle T_1\rangle$. A grid search was used to obtain an initial guess of the other model-free parameters with τ_m held constant. Then the model-free parameters were optimized by minimizing χ^2 given by

$$\chi^2 = \sum_i \frac{(R_{1i}{}^e - R_{1i}{}^c)^2}{\sigma_{1i}{}^2} + \frac{(R_{2i}{}^e - R_{2i}{}^c)^2}{\sigma_{2i}{}^2} + \frac{(NOE_i{}^e - NOE_i{}^c)^2}{\sigma_{NOEi}{}^2}$$

in which $R_{1i}{}^e$, $R_{2i}{}^e$, and $NOE_i{}^e$ are the corresponding experimental values of the relaxation parameters; and σ_{1i}, σ_{2i}, and σ_{NOEi} are the corresponding experimental uncertainties in the relaxation parameters. $R_{1i}{}^c$, $R_{2i}{}^c$, and $NOE_i{}^c$ are the calculated values. The quality of the fit between the experimental data and theoretical models was assessed by comparing the optimal values of χ^2 with the $\alpha = 0.05$ critical value of the distribution of χ^2 determined from Monte Carlo simulations. During this step, five motional models were evaluated and one was selected. Following the determination of the appropriate model for each amide, the overall correlation time was optimized for all of the residues simultaneously. Once the global optimal τ_m value was determined, the relaxation parameters were fitted again using the selected model.

Calculation of the Rotational Diffusion Tensor. The degree of anisotropy was determined using two methods, from direct fitting of T_1/T_2 ratios and from the local diffusion constants as described previously (*38*−*40*) using the programs kindly provided by Professor Arthur G. Palmer, III. Residues with no conformational exchange and nanosecond internal motions were used for calculation of the diffusion tensor of UBC9. Direct fitting of T_1/T_2 ratios assumed that the molecule has an axially symmetrical top. Local diffusion constants were also used to calculate the rotational diffusion tensor. These

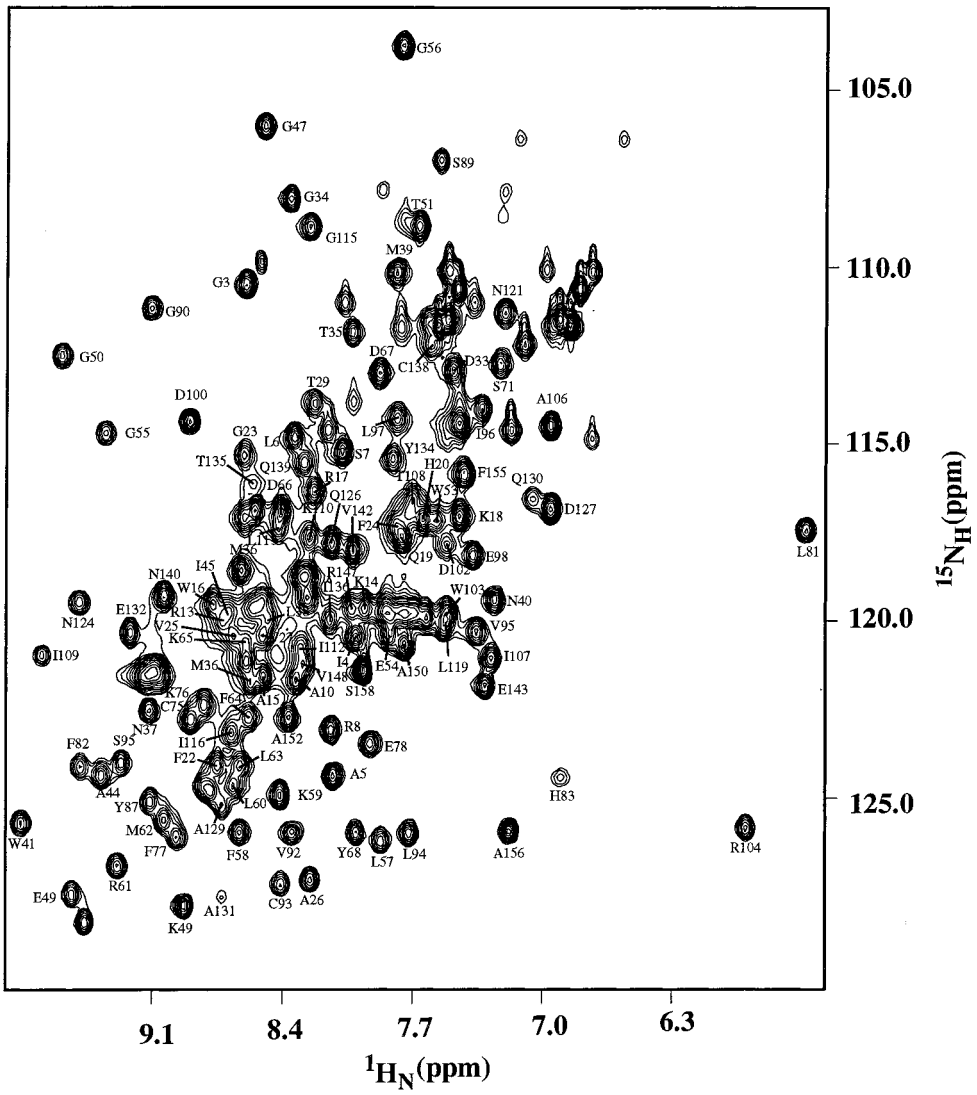

FIGURE 1: ^{1}H-^{15}N HSQC of UBC9. Residues that were used for dynamic studies are labeled in the spectrum.

data were fit to three diffusion models: isotropic, axially symmetric, and fully anisotropic. F-statistical testing was used to select the model which best represented the rotational diffusion of UBC9. Coordinates of the crystal structure of UBC9 (*24*) were used for the analysis.

RESULTS

^{15}N Relaxation Measurements. ^{15}N T_1^{-1}, T_2^{-1}, and ^{1}H-^{15}N NOE relaxation rates were measured at 0.7 mM protein concentration. ^{15}N T_1^{-1} and T_2^{-1} rates were also measured at 0.3 mM protein concentration. These relaxation rates were obtained for 111 out of the 143 residues (excluding 15 prolines) which can be observed in the ^{1}H-^{15}N HSQC spectrum. These residues are labeled in the HSQC spectrum in Figure 1. The residues that were not measured have severe resonance overlaps, so that the intensities of their ^{1}H-^{15}N cross-peaks cannot be estimated accurately. The ^{15}N T_1^{-1}, T_2^{-1}, and ^{1}H-^{15}N NOE of UBC9 backbone resonances are shown in Figure 2. For samples with 0.7 mM protein concentration, the average nitrogen longitudinal relaxation rates and transverse relaxation rates were 1.26 ± 0.06 and 17.7 ± 0.6 s^{-1}, respectively, and the average ^{15}N− ^{1}H steady-state NOEs were 0.74 ± 0.03 s^{-1}. For the sample with 0.3 mM protein concentration, the average ^{15}N T_1^{-1} and T_2^{-1} were 1.45 ± 0.17 and 15.5 ± 1.2 s^{-1}, respectively.

The Overall Rotational Correlation Time. The overall correlation time, τ_m, was initially estimated from the average value of T_1/T_2 of 91 residues. The amide relaxation of these residues was expected to be dominated by fast internal motions. The estimated τ_m was 14.02 ± 0.06 ns. The final optimized overall correlation time during the model-free analysis of all ^{15}N T_1, T_2, and {^{1}H-^{15}N} NOE data was 14.07 ± 0.06 ns. This τ_m value appears to be larger than that expected from the size and the crystal structure of UBC9. Thus ^{15}N T_1^{-1} and T_2^{-1} were measured again using a 0.3 mM UBC9 sample in order to determine whether UBC9 is partially associated with each other at these concentrations. The apparent rotational correlation time at 0.3 mM is 12.03 ± 0.13. These data suggest that UBC9 partially aggregates. If the protein undergoes dimer−monomer equilibrium, the dissociation constant, estimated from the apparent rotational correlation times at the two concentrations, is approximately 1.2 mM.

Diffusion Anisotropy. UBC9 is an anisotropic molecule with the ratio of the principal axes of the inertia tensor calculated from the crystal structure being 2.284:2.0158:1.

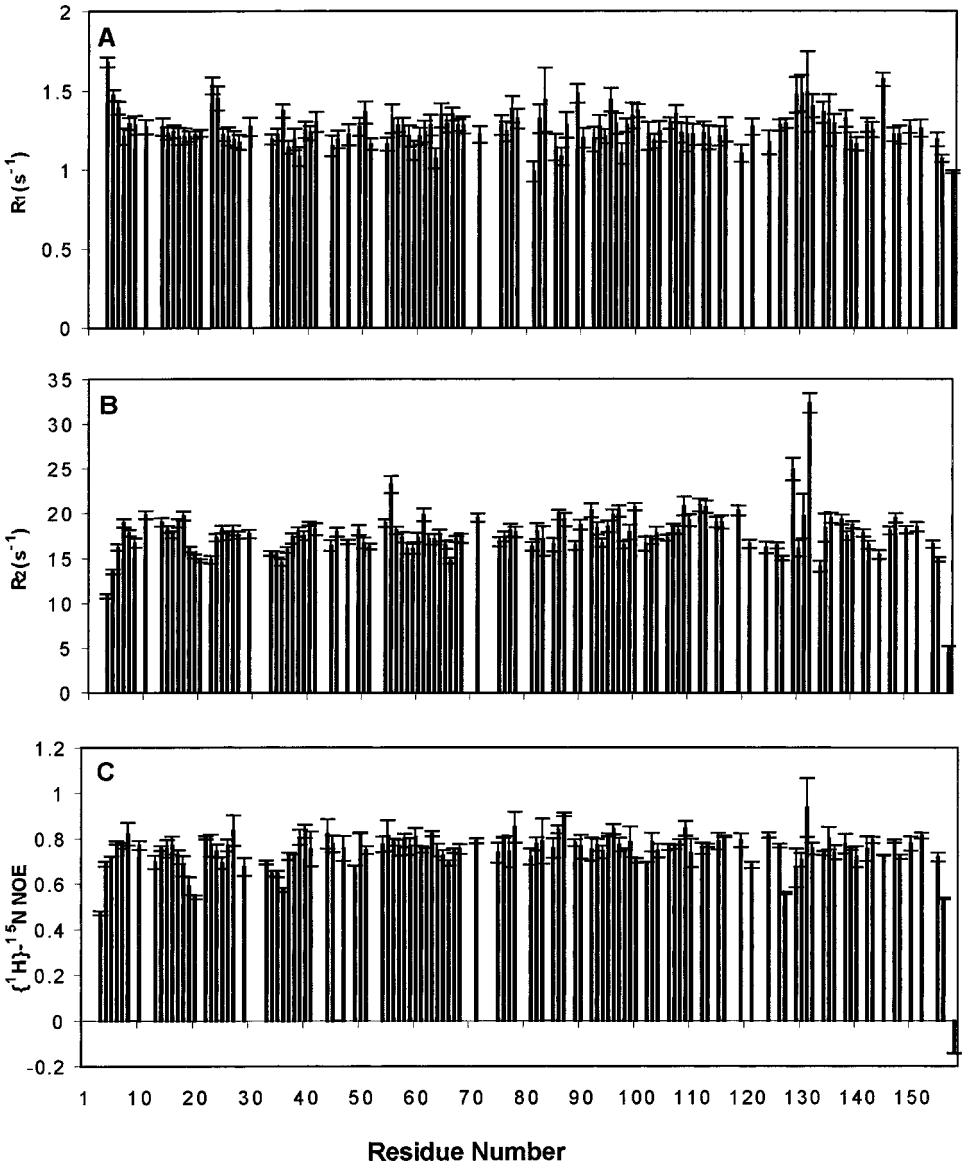

FIGURE 2: Plots as a function of residue number of (a) ^{15}N T_1^{-1}, (b) T_2^{-1}, and (c) ^{1}H-^{15}N NOE of UBC9. Only residues whose ^{1}H-^{15}N cross-peaks are resolved enough to permit accurate measurements of their intensities are included.

However, the anisotropy is relatively small from the analysis of the T_1/T_2 ratio. The T_1/T_2 ratio is related to $Y_2°$ as follows:

$$T_{1i}/T_{2i} = (T_{1i}/T_{2i})_{iso}[1 + 2Y_2°(\theta_i)(D_{||}/D_{\perp})/3]$$

where $(T_{1i}/T_{2i})_{iso}$ is the result using $D_{iso} = \text{trace}\{\mathbf{D}\}/3$. The experimental and least-squares fitted T_1/T_2 ratios versus $Y_2°$ are shown in Figure 3. This figure shows that the NH bond vectors are reasonably well distributed to allow a good estimation of the diffusion tensor. The diffusion tensor of the protein has been estimated with both direct fitting of T_1/T_2 ratios and calculation from local diffusion constants estimated from T_1/T_2 ratios (*38*−*40*). The calculation using local diffusion constants was performed for three models: isotropical rotational diffusion, axially symmetrical rotational diffusion, and axially asymmetric rotational diffusion. Based on F-statistical testing, the axially symmetrical model can represent the diffusion well. An axially asymmetric model, statistically, does not give better fitting to the experimental data. The calculation of the diffusion tensor by directly fitting T_1/T_2 ratios used the axially symmetrical model. Both methods gave similar results, and the difference was within experimental error. The diffusion tensor of UBC9 has the ratio $D_{||}/D_{\perp}$ of 1.18 ± 0.03. The His-tag at the N-terminus contains 8 amino acids with random conformation which may reduce the diffusion anisotropy slightly. Partial dimerization can also change the diffusion anisotropy. The *z*-axis of the diffusion tensor is nearly parallel to α-helix 2 and is approximately 8° ± 5° away from the shortest axis of the inertia tensor.

Model-Free Approach. The model-free approach (*35*, *36*) was used to obtain quantitative information about internal motions of proteins from NMR relaxation measurements. UBC9 was assumed to undergo isotropic rotational diffusion for obtaining model-free parameters. Assuming isotropic rotational diffusion for anisotropic molecules can result in artifacts in model-free parameters. Significant artifacts are found in conformational exchange terms (R_{ex}) and nanosecond internal motions. Some errors in S^2 can also occur; however, the overall trend in S^2 should not be affected (*41*). Both theoretical and experimental results have shown that

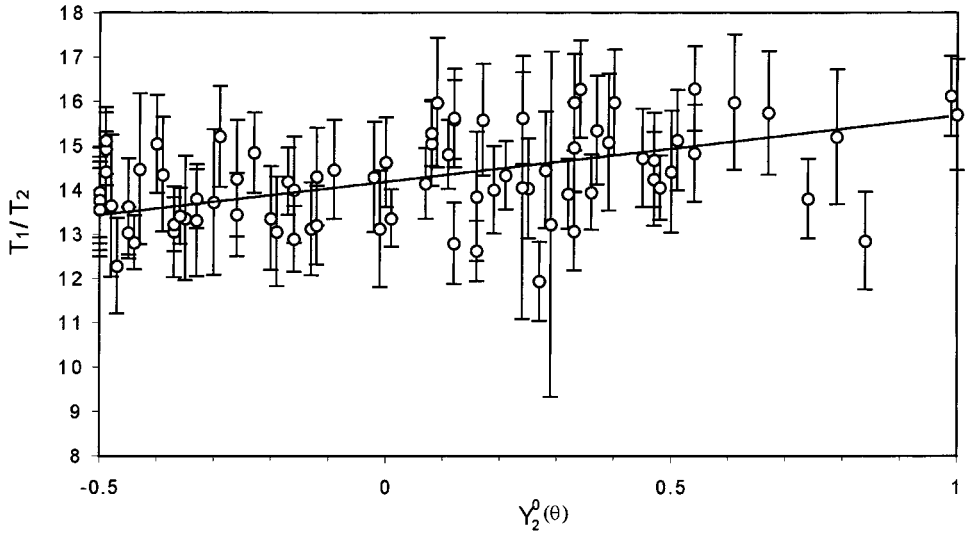

FIGURE 3: Plots of T_1/T_2 ratio versus $Y_2°$ of each NH bond vector showing the angular distribution of NH bond vectors used for calculation of the rotational diffusion tensor.

most of the model-free parameters can be obtained with reasonable accuracy by assuming isotropic rotation when the anisotropy is small ($D_{\parallel}/D_{\perp} < 2$). The ^{15}N relaxation rates of 107 residues could be well fit to the model-free or the extended model-free formalism with χ^2 values smaller than the 95% critical value, while the remaining four residues (22, 50, 87, and 145) could not. The model-free parameters are shown in Figure 4.

Model-free analysis also shows that UBC9 is, overall, a rigid molecule. Other than the N- and C-termini, all S^2 values are higher than 0.7, including all loops. The terminal residues 3, 4, and 158 have S^2 values below 0.7. The loop regions have relatively higher flexibility. Residues Asp[19], His[20], Asp[33], Gly[34], Thr[35], Met[36], Leu[38], Asp[66], Leu[81], Val[86], Ser[89], Leu[97], Leu[119], Asp[127], Gln[130], Tyr[134], and Ala[156] have S^2 values between 0.7 and 0.85. The residues with S^2 less than 0.85 are color-coded on the three-dimensional structure of UBC9 in Figure 5A. With the exception of residues 97 and 134, all of these residues are located in turns and loops between the secondary structures. Residue 134 is located in a short α-helix and 97 is located in a short 3_{10} helix. The residues in secondary structural regions have higher S^2 values, indicating that they are more rigid. With the exception of the first four residues of helix 1 at the N terminus, which have S^2 less than 0.7, most S^2 values for the residues in secondary structures are relatively uniform and higher than 0.9. The average S^2 values in α-helix 1−4 are 0.88, 0.94, 0.93, and 0.95, respectively. The four β strands have average S^2 values of 0.92, 0.92, 0.91, and 0.95, respectively. The uniformly large values indicate that this molecule is quite rigid; the surface loops are also of limited flexibility.

Information on the time scales of internal motions that are faster than the overall correlation time are given by τ_e. Most residues have τ_e less than 200 ps, indicating that the internal motions are fast. Fourteen residues show relatively slower internal motions. These residues are in helix 1 (Gly[3], Ile[4], and Ala5), loops (Asp[19], His[20], Thr[35], Asp[66], Ser[89], Glu[98], Gln[126], Asp[127], and Gln[130]), and α-helixes 3 and 4 (Tyr[134] and Ser[158]), and are indicated in the three-dimensional structure of UBC9 in Figure 5B. The τ_e values in these residues are approximately 1−4 ns. In anisotropic molecules, the NH bond vectors, which lie along the *x*-axis of the diffusion tensor, have the smallest T_1/T_2 ratio. This may result in an artificially slow internal motion, if an isotropical model is used for fitting the relaxation data. In twelve residues of UBC9, the angles between the NH bond vector and the unique axis are between 80° and 100°. Only three residues, Asp[66], Ser[89], and Gln[127], show slow internal motions with τ_e's of 2 ± 0.2, 4.5 ± 1.5, and 1.1 ± 0.1 ns, respectively. The NH vectors of the three residues have different orientations relative to one another. Other residues do not require τ_e or R_{ex} for data fitting. The average T_1/T_2 ratio of the other 9 residues is 14.0 which is similar to the average T_1/T_2 ratio for all residues (14.1 ± 0.2). Therefore, the slow internal motions in these three residues are not likely to be an artifact from data fitting due to the assumption of isotropic overall rotational diffusion. Most of these residues have smaller S^2, consistent with higher conformational flexibility in these regions.

Twenty-three residues appear to have internal motions on the time scales of microseconds to milliseconds indicated by the R_{ex} terms. These residues are Leu[6], Ala[10], Arg[13], and Arg[17] in helix 1; Leu[38], Glu[54], Gly[55], Ser[71], Leu[81], Val[86], Val[92], Asp[100], Ala[129], Glu[132], and Asn[140] in loops; Ile[109], Ile[112], Leu[113], and Leu[119] in α-helix 2; Ile[136] in α-helix 3; Val[148] in α-helix 4; Arg[61] in a β-strand; and Leu[97] in a 3_{10} helix. Gln[132] has the highest R_{ex} value of 14.7 s^{-1} and a S^2 value of 0.72. Molecules with anisotropic overall rotational diffusion will have the largest T_1/T_2 ratios for those NH bond vectors which are parallel to the unique axis. Three residues in UBC9, Leu[38], Gly[115], and Asn[140] have NH bond vectors oriented less than 10° from the unique axis of the molecule. All three residues have larger values of the ratio T_1/T_2 (with an average of 16.1) compared to the average of 14.1. The chemical exchange terms of these three residues are likely to be artifacts due to using an isotropic model for data analysis. The residues which have the largest R_{ex} term (>4 s^{-1}) are Gly[55], Val[86], Leu[97], Leu[119], Ala[129], and Gln[132]. These residues, except Gly[55] and Glu[132], are adjacent to the active site Cys[93] as shown in Figure 5C.

Reduced Spectra Density Mapping. Reduced spectra density mapping (for a review, see ref *29*) is an alternative

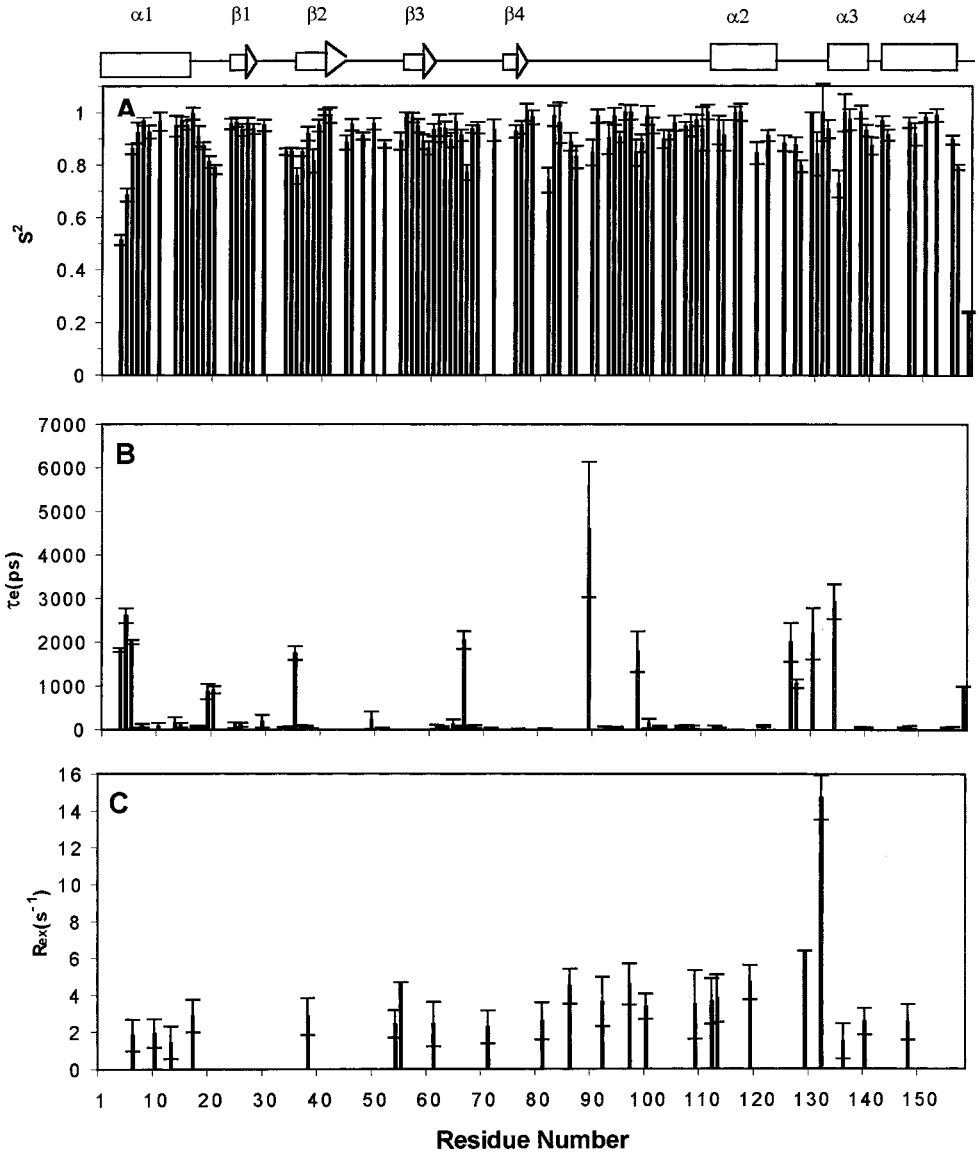

FIGURE 4: Plots as a function of residue number of (a) S^2, (b) τ_e, and (c) R_{ex} of UBC9. Only residues whose ^{1}H-^{15}N cross-peaks are resolved enough to permit accurate measurements of their intensities are included.

method which can be used to obtain information about dynamics without assuming any model for internal motion. From ^{15}N T_1^{-1}, T_2^{-1}, and ^{1}H-^{15}N NOE measurements, spectral density functions $J_{eff}(0)$, $J(\omega_N)$, and $J(\omega_H)$ were calculated and are shown in Figure 6. $J_{eff}(0)$ is sensitive to chemical exchange processes since it is dominated by T_2^{-1}, whereas $J(\omega_H)$ is sensitive to fast internal motions on the nanosecond to picosecond time scales. In addition to internal motions, rotational diffusion anisotropy can also cause variations in spectral density functions (*42*). For UBC9, the diffusion anisotropy was estimated to cause less than 10% variation in spectral density functions. In the absence of internal motions, the NH bond vectors which are parallel to the unique axis have the largest $J(0)$, but smallest $J(\omega_N)$ and $J(\omega_H)$. For the NH bond vectors, which are perpendicular to the unique axis, $J(0)$ is the smallest but $J(\omega_N)$ and $J(\omega_H)$ are the largest.

Residues with larger or smaller $J(0)$ were analyzed. Residues that have $J(0)$ more than 0.5×10^{-9} s^{-1} smaller than the average value of $J(0)$, 5.36×10^{-9} s^{-1}, all have S^2 values less than 0.85, except the three residues 18, 22, and 145. The range $\pm 0.5 \times 10^{-9}$ s^{-1} is larger than 10% of the average value of $J(0)$ and should include the variation in $J(0)$ caused by rotational diffusion anisotropy. Residues 18, 22, and 145 cannot be fitted using the model-free or the extended model-free approach with χ^2 values smaller than the 95% critical value. Few residues, 38, 81, 86, 97, and 119, have S^2 values smaller than 0.85, but are within the range of $5.36 \times 10^{-9} \pm 0.5 \times 10^{-9}$ s^{-1}. All of these residues have a large R_{ex} term, as analyzed from the model-free approach. In UBC9, $J(0)$ is quite sensitive to large amplitude internal motions on the picosecond to nanosecond time scales if the residue does not have conformational exchange.

Residues that have $J(0)$ more than 0.5×10^{-9} s^{-1} larger than 5.36×10^{-9} s^{-1} all have an R_{ex} term from the model-free analysis, except residues 96, 131, and 138. Several residues, 6, 13, 38, 54, 81, and 140, have R_{ex} terms by model-free analysis, but are within the range of $5.36 \times 10^{-9} \pm 0.5 \times 10^{-9}$ s^{-1}. The R_{ex} values of these residues range from 1.8 to 2.8 s^{-1}. Larger values of $J(0)$ indicate chemical exchange processes, whereas smaller $J(0)$ values correlate to large amplitude fast internal motions. For the residues whose NH

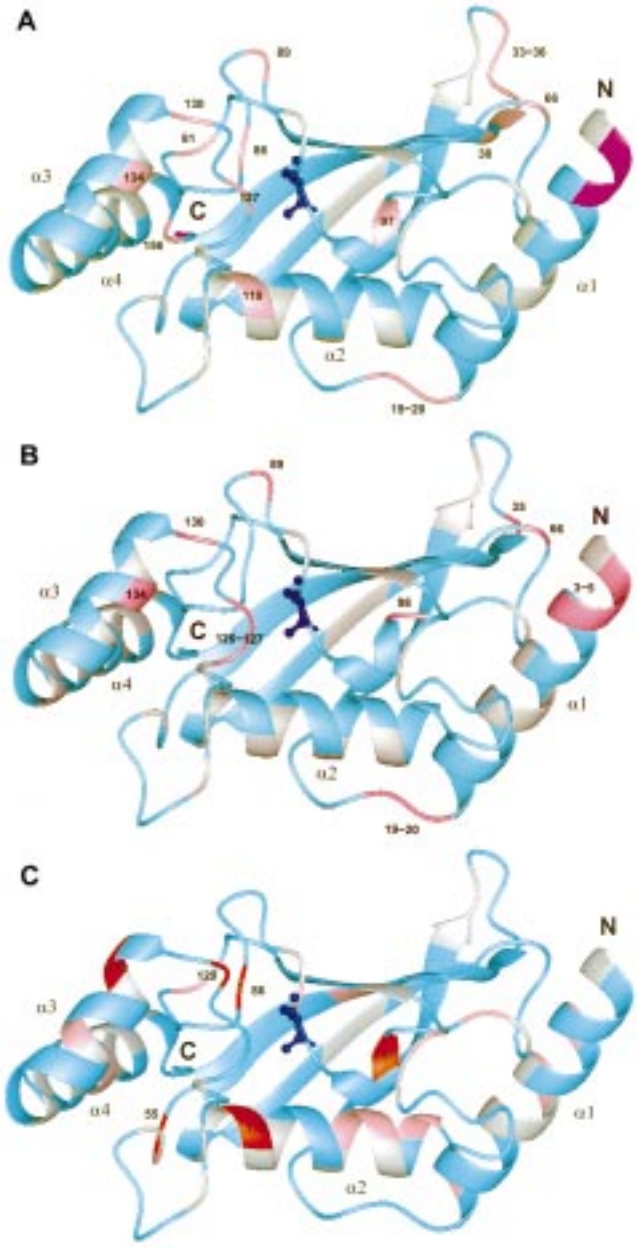

FIGURE 5: The structure of UBC9 is color-coded according to the model-free parameters. (A) The structure is color-coded according to S^2 values. Purple indicates residues that have $S^2 < 0.7$; pink indicates residues that have $0.7 < S^2 < 0.85$. Residues with $0.7 < S^2 < 0.85$ are indicated with their amino acid sequence numbers. (B) The structure is color-coded with τ_e. Residues with $\tau_e > 700$ ps are indicated with pink and with their residue numbers. (C) The structure is color-coded with R_{ex}. Residues with $0 < R_{ex} < 4$ s^{-1} are indicated with pink, and residues with $R_{ex} > 4$ s^{-1} are indicated with red and their residue numbers. In all three panels, gray indicates residues for which resonances are too overlapped in the ^{1}H-^{15}N HSQC spectrum to permit accurate measurements of their intensities. The side chain of active site Cys^{93} is shown in these figures. Four α-helices are labeled with α1−4.

bond vectors are parallel to the unique axis of the diffusion tensor, $J(0)$ was not significantly larger, whereas the model-free approach resulted in a significant R_{ex} term.

$J(\omega_H)$ has also been compared with the model-free parameters. Twelve out of 19 residues which have S^2 values less than 0.85 have $J(\omega_H)$ values more than 1×10^{-12} s^{-1} larger than the average value, 5.06×10^{-12} s^{-1}. The residues that did not show significant larger $J(\omega_H)$ values but have smaller S^2 values are 33, 38, 81, 86, 89, 97, 119, and 134 with S^2 values ranging from 0.73 to 0.85. Some residues, such as 5, 18, 29, 49, 100, 121, 129, and 145, which have S^2 values larger than 0.85, also show $J(\omega_H)$ values larger than 6.0×10^{-12} s^{-1}. Significantly smaller values of $J(\omega_H)$ do not correlate to either fast internal motions or chemical exchange processes determined from the model-free approach. The fact that $J(\omega_H)$ is less sensitive to large amplitude fast internal motions than $J(0)$ may result from larger errors in the estimation of $J(\omega_H)$.

Amide Proton Exchange Studies. Exchange of amide protons with solvent D_2O in UBC9 provided information on the stability of hydrogen-bonded secondary structures. Exchange rates are color-coded in the structure of UBC9 in Figure 7. Helix 1 (residues 1−18) is the most flexible helix with most of the amide protons, particularly the first 9 residues, exchanging completely with solvent D_2O in less than 0.5 h. The β-sheet is highly stable with most of the amide protons involved in interstrand H-bonding remaining unexchanged with D_2O for more than 15 h. The helix encompassing residues 109−121 (α2) is also very stable, characterized by the fact that most amide protons were not being exchanged with solvent for more than 15 h. The remaining two helices encompassing residues 133−139 and residues 141−155 are less stable, with many amide protons exchanged between 4 and 15 h. Most residues in the loop and turn regions exchange fast with solvent. Several residues in loop regions, such as residues 85−87, have stable amide protons. These residues are buried or partially buried in the structure of UBC9.

DISCUSSION

Dimerization and the Effect on S^2. Self-association in UBC9 has been suggested from ^{15}N T_2^{-1} measurements at two different concentrations. This may be due to nonspecific aggregation at the concentration required for NMR studies, or due to specific self-interactions. Self-interactions of E2 and interactions among E2 enzymes have been demonstrated and have been indicated to play important roles in their functions. For example, it has been suggested that the functions of UBC3 (CDC34) depend on interactions with another UBC3 or the DNA repair enzyme UBC2 (RAD6) (*43*). It was found that the turnover of yeast Matα2 transcription factor is strongly correlated with the interaction of UBC6 and UBC7 (*44*). In addition, UBC7, UBC4, and UBC3 have been demonstrated to interact with themselves in a specific manner (*45*, *46*). Self-interaction and interactions among E2 enzymes may be one mechanism to regulate substrate specificity. Dimerization in UBC9 was not observed previously, since most biochemical approaches cannot detect weak interactions easily. Rotational diffusion anisotropy is sensitive to weak self-associations. ^{15}N T_1^{-1} and T_2^{-1} measurements have shown that UBC9 interacts weakly with itself under the conditions of our NMR study.

The generalized order parameter S^2 of UBC9 is, on average, slightly higher than most proteins, particularly for residues that are in secondary structural regions. Seventy-two out of the 107 residues have S^2 values greater than or equal to 0.90. Twenty-five residues have S^2 values between 0.8 and 0.9. Ten residues have S^2 smaller than 0.8. The overall higher S^2 is likely to result from partial dimerization of UBC9 during NMR studies. It has been shown, in a

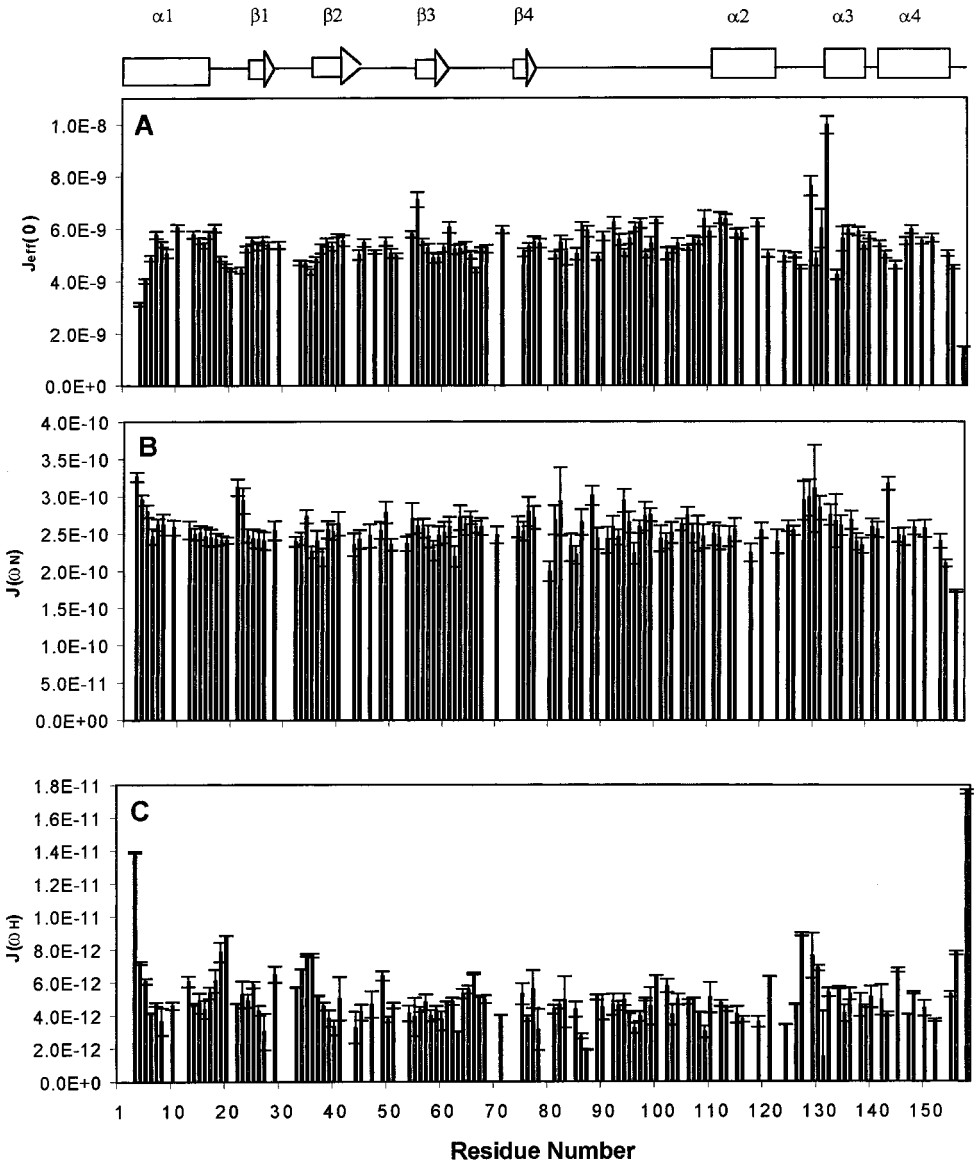

FIGURE 6: Plots of reduced spectral density functions (a) $J(0)$, (b) $J(\omega_H)$, and (c) $J(\omega_N)$ versus residue number.

theoretical simulation, that when a molecule undergoes dimer-monomer equilibrium, S^2 obtained by fitting relaxation data may slightly exceed the actual S^2, even when a system contains 10% dimer and 90% monomer (*41*). However, the source of this error was not explained. We examined the effect of using a single correlation time to represent the mixture of monomer and dimer. If the exchange rate of the monomer−dimer equilibrium is faster than the relaxation rates but slower than that of the overall tumbling, the spectral density of the mixture of monomer and dimer is the population-weighted average (*47*). Thus the average overall correlation time estimated from T_1^{-1}, which is dominated by $J(\omega_N)$, is a population-weighted average of $1/\tau$, that is, $\langle 1/\tau \rangle$. However, the average correlation time estimated from T_2^{-1} is a population-weighted average of τ, that is, $\langle \tau \rangle$, since T_2 is dominated by $J(0)$. Using a single correlation time to fit the model-free parameters for a system with monomer−dimer equilibrium provides an overall correlation time from $(\langle \tau \rangle / \langle 1/\tau \rangle)^{1/2}$. This overall correlation time is smaller than $\langle \tau \rangle$ but larger than $1/\langle 1/\tau \rangle$. When this average correlation time is used to fit model-free parameters, S^2 needs to be increased to compensate for the decrease in τ for the spectral density

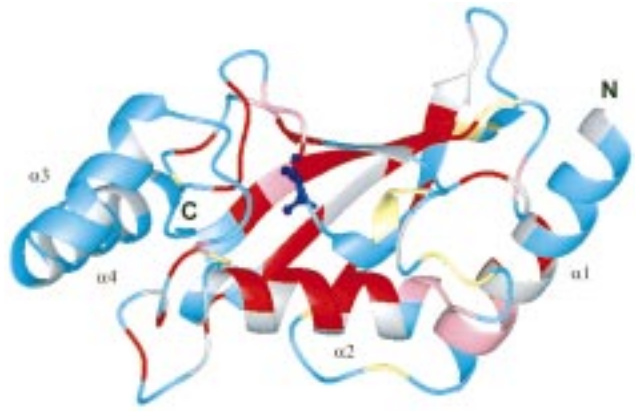

FIGURE 7: The structure of UBC9 is color-coded with ^{1}H-^{2}H exchange rates. Residues that have lifetimes longer than 15 h are indicated in red, those have lifetimes between 4 and 15 h are shown in pink, those with lifetimes between 0.5 and 4 h are shown in yellow, and those with lifetimes too fast to be detected (<0.5 h) are shown in cyan. Gray indicates residues for which resonances are too overlapped in the ^{1}H-^{15}N HSQC spectrum to permit accurate measurements. The side chain of active site Cys^{93} is shown in the figure. Four α-helices are labeled with α1−4.

function $J(0)$ and decrease of $1/\tau$ for other spectral density functions. Thus, the S^2 obtained using a single rotational correlation time for a protein udergoing monomer and dimer equilibrium will be slightly increased, but the trend in S^2 should not be affected significantly.

Conformational Flexibility. Both ^{15}N-relaxation and amide proton exchange studies suggest that the flexible regions of human UBC9 are localized at the N- and C-termini. The two regions are located at opposite sides of the active site Cys^{93}. The central portion which contains the β-sheet and α-helix 2 is the most stable region, characterized by the slowest exchanging amide protons and the absence of internal motions on the nanosecond to millisecond time scales. The first and the last two helices are less stable with most of the amide protons exchanged in D_2O within 15 h.

The residues undergoing large amplitude internal motions on the picosecond to nanosecond time scales are localized around two regions on the same face where the active site Cys^{93} residue is located. The first region is around the N-terminus. The N-terminal helix is the most flexible secondary structure in human UBC9. In particular, the first 8 residues are highly mobile with low S^2 values, nanosecond τ_e values and fast exchanging amide protons. Three loops at residues 35, 66, and 100 are close to the N-terminal helix in the three-dimensional structure. In addition, residues 19 and 20 which connect the first helix to the β-sheet also have higher flexibility (Figure 5A,B).

The second region of higher conformational flexibility is located on the C-terminal side of Cys^{93} (Figure 5A,B). This region consists of several surface loops, the C-terminal end of helix 2, and helix 3 including residues Leu^{81}, Val^{86}, Ser^{89}, Leu^{97}, Leu^{119}, Gln^{126}, Asp^{127}and Ala^{129}, Gln^{130}, and Glu^{132}. A difference in this region from the N-terminal flexible region is the substantial conformational exchange (Figure 5C). In particular, one of the residues in this region, Glu^{132}, has the largest chemical exchange term (13.8 s^{-1}) in the whole protein.

Residues undergoing conformational exchange surround the active site. Residues Gly^{55}, Val^{86}, Leu^{97}, Leu^{119}, Ala^{129}, and Glu^{132} have the largest chemical exchange terms (>4 s^{-1}) and are in the vicinity of the active site Cys^{93} (Figure 5C). Some residues in the vicinity, Leu^{81}, Ser^{89}, Gln^{126}, Asp^{127}, and Gln^{130}, have higher than average flexibility on the picosecond to nanosecond time scales. The side chain of residue Asp^{127} orients itself toward the ubiquitin accepting sulfhydryl group. This residue may play a critical role in UBC9's catalytic activity.

Substrate Binding. An E2 enzyme can recognize diverse substrate proteins, although each E2 enzyme has its own specificity. Protein−protein recognition requires large numbers of specific interactions including H-bonds, hydrophobic interactions, and salt bridges. This is achieved, in some cases, through structurally complimentary surfaces between the interacting partners. In other cases, one molecule is more flexible and can be induced to fit the surface of the other protein. Since an E2 enzyme can recognize a wide range of substrate proteins, adjustment of its conformation may be required to fit a range of different contact surfaces. Thus, multiple conformations at the substrate binding site on E2 should be accessible energetically, suggesting that the substrate binding site is likely to have higher conformational flexibility.

Two regions of higher flexibility on UBC9 have been identified in this study. The region near the N-terminus is not likely to be the substrate binding site. The N-terminus of *Arabidopsis* UBC1 has been shown to interact with E1−ubiquitin conjugate (*28*). Due to high sequence and functional similarities, the N-terminus of UBC9 may also be involved in interaction with the E1−UBL1 conjugate. The two loops at residues 35 and 100, which are highly variable in the amino acid sequences and three-dimensional structures between different E2 enzymes, are close to the N-terminal helix. This spatial proximity suggests that they may be involved in recognition of E1−ubiquitin conjugate, but not substrate proteins. The structural variation of these two loops may be important for UBC9's specificity to UBL1 (a ubiquitin homologue) and/or E1 protein specific for UBL1 and UBC9. The E1 homologue which activates a ubiquitin-like molecule for conjugation to UBC9 has recently been identified in yeast (*15*). Flexibility in this region may be responsible for equilibrium binding of the E1−ubiquitin conjugate.

The second more flexible region may play an important role in substrate binding. This region is close to the C-terminus, which was shown to interact with substrate proteins in wheat UBC4 (*48*). The C-terminal helix also has a positive electrostatic potential. Sequence analysis of proteins which interact with UBC9 indicates that they mostly have a region of strong overall negative charge (*24*), which can be attracted to the electrostatic positive C-terminus of UBC9. The second more flexible region forms a surface which contains many hydrophobic residues. Hydrophobic interactions may play important roles in interactions of UBC9 with other proteins, as it was shown previously that the interaction between UBC9 and the *Adenovirus* E1A protein is affected by a single Leu to Ile substitution on E1A. Since this region is also close to the active site Cys^{93}, the conformational flexibility may also play critical roles in the catalytic activity of transferring the C-terminus of ubiquitin (UBL1 for this system) to a Lys residue on a substrate protein.

UBC9 is a relatively rigid molecule. None of the surface loops are flexible enough to allow large scale conformational changes. Substrate specificity and diversity are not likely to be conferred solely by UBC9 itself. UBL-1, which is homologous to ubiquitin and specific to UBC9, may participate in recognizing the specific substrate proteins. Thus substrate specificity in E2 enzymes may not only depend on structural variations in E2 enzyme, but also depend on different ubiquitin-like proteins which conjugate to different E2 enzymes. UBL-1 may also have regions that are highly flexible in the three-dimensional structure which can be adjusted to fit different substrate proteins upon binding. Since UBC9 belongs to class I E2 molecules which lack the C-terminal extension in the amino acid sequence, an E3 protein may also be involved in substrate binding, although the E3 protein related to UBC9 has not been found and it is not clear whether an E3 is required in this system.

In conclusion, we have identified two regions in human UBC9 which show higher mobility over a wide range of time scales than other regions of the protein. Combined with previous biochemical studies, both regions are likely to be important for protein−protein recognition in the ubiquitin pathway. The region near the N-terminus may be important

for interactions with E1-ubiquitin conjugate. The region near the C-terminus, which is the most flexible on microsecond to millisecond time scales, may be important for substrate binding and catalytic activity. It is likely that the substrate binding site on E2 is close to the catalytic active site, since the C-terminus of a ubiquitin or ubiquitin-like protein needs to be transferred from E2 to substrate proteins. Since E2 enzymes share high homology in primary sequences and three-dimensional structures, the conformational flexibility of UBC9 may represent a general feature of E2 enzymes. This study should provide a new perspective for further studies of protein−protein recognition in ubiquitination.

ACKNOWLEDGMENT

We thank Dr. Arthur G. Palmer, III for the computer programs used to analyze the relaxation data and for helpful discussions. We also thank Drs. Benoit Boulat, David Fushman, Xiubei Liao, Zhiyuan Shen, and Martin J. Stone for helpful discussions.

REFERENCES

1. Jentsch, S. (1992) *Annu. Rev. Genet. 26*, 179−207.
2. Hass, A. L., and Siepmann (1997) *FASEB J. 11*, 1257−1268.
3. Varshavsky, A. (1997) *Trends Biochem. Sci. 22*, 383−387.
4. Seufert, W., Futcher, B., and Jentsch, S. (1995) *Nature 373*, 78−81.
5. Barinaga, M. (1995) *Science 269*, 631−632.
6. Pagano, M., Tam, S. W., Theodoras, A. M., Beer-Romero, P., Del Sal, G., Chau, V., Yew, P. R., Graetta, G. F., and Rolfe, M. (1995) *Science 269*, 682−685.
7. Haas, A. L., Baboshina, O., Williams, B., and Schwartz, L. M. (1995) *J. Biol. Chem. 270*, 9407−9412.
8. Wiebel, F. F., and Kunau, W. H. (1992) *Nature 359*, 73−76.
9. Finley, D. and Chau, V. (1991) *Annu. Rev. Cell Biol. 7*, 25−69.
10. Sommer, T., and Jentsch, S. (1993) *Nature 365*, 176−179.
11. Saitoh, H., Pu, R. T., and Dasso, M. (1997) *Trends Biochem. Sci. 22*, 374−376.
12. Haas, A. L., Ahrens, P., Bright, P. M., and Ankel, H. (1987) *J. Biol. Chem. 262*, 11315−11323.
13. Kumar, S., Yoshida, Y., and Noda, M. (1993) *Biochem. Biophys. Res. Commun. 195*, 393−399.
14. Caliis, J., Carpenter, T., Sun, C. W., and Viestra, R. D. (1995) *Genetics 139*, 921−939.
15. Johnson, E. S., Schwienhorst, I., Dohmen, R. J., and Blobel, G. (1997) *EMBO J. 16*, 5509−5519.
16. Seufert, W., and Jentsch, S. (1990) *EMBO J. 9*, 543−550.
17. Seufert, W., McGrath, J. P., and Jentsch, S. (1990) *EMBO J. 9*, 4535−4541.
18. Shen, Z., Pardington-Purtymun, P. E., Comeaux, J. C., Moyzis, R. K., and Chen, D. J. (1996) *Genomics 37*, 183−186.
19. Al-Khodairy, F., Enoch, T., Hagan, I. M., and Carr, A. (1995) *Am. J. Cell Sci. 108*, 475−486.
20. Gottlicher, M., Heck, S., Doucas, B., Wade, E., Kullmann, M., Cato, A. C. B., Evans, R. M., and Herrlich, P. (1996) *Steroids 61*, 257−262.
21. Wang, Z. Y., Qui, Q. Q., Seufert, W., Taguchi, T., Testa, J. R., Whitmore, S. A., Callen, D. F., Welsh, W., Shenk, T., and Deuel, T. G. (1996) *J. Biol. Chem. 271*, 24811−24816.
22. Yasugi, T., and Howley, P. (1996) *Nucleic Acids Res. 24*, 2005−2010.
23. Hateboer, G., Hijmans, E. M., Nooij, J. B. D., Schlenker, S., Jentsch, S., and Bernards, R. (1996) *J. Biol. Chem. 271*, 25906−25911.
24. Tong, H., Hateboer, G., Perrakis, A., Bernards, R., and Sixma, T. K. (1997) *J. Biol. Chem. 272*, 21381−21387.
25. Cook, W. J., Jeffrey, L. C., Sullivan, M. L., and Vierstra, R. D. (1992) *J. Biol. Chem. 267*, 15116−15121.
26. Cook, W. J., Jeffrey, L. C., Xu, Y., and Chau, V. (1993) *Biochemistry 32*, 13809−13817.
27. Cook, W. J., Martin, P. D., Edwards, B. F. P., Yamazaki, R. K., and Chau, V. (1997) *Biochemistry 36*, 1621−1627.
28. Sullivan, M. L., and Vierstra, R. D. (1991) *J. Biol. Chem. 266*, 23878−23885.
29. Dayie, K. T., Wagner, G., and Lefèvre, J. F. (1996) *Annu. Rev. Phys. Chem. 47*, 243−282.
30. Englander, J. J., Englander, S. W., Louie, G., Roder, H., Tran, T., and Wand, A. J. (1988) *Protein hydrogen exchange, dynamics, and energetics. in Structure & Expression, Volume 1: From Proteins to Ribosomes* (Sarma, R. H., and Sarma, M. H., Eds.), pp 107−117.
31. Liu, Q., Shen, B. H., Chen, D. J., and Chen, Y. (1998) *J. Biomol. NMR* (in press).
32. Farrow, N. A., Muhandiram, R., Singer, A. U., Pascal, S. M., Kay, C. M., Gish, G., Shoelson, S. E., Pawson, T., Forman-Kay, J. D., and Kay, L. E. (1994) *Biochemistry 33*, 5984−6003.
33. Jones, J. A. (1997) *J. Magn. Reson. 126*, 282−286.
34. Abragam, A. (1961) *Principles of Nuclear Magnetism*, Clarendon Press, Oxford, U.K.
35. Clore, G. M., Szabo, A., Bax, A., Kay, L. E., Driscoll, P. C., and Gronenborn, A. M. (1990) *J. Am. Chem. Soc. 112*, 4989.
36. Lipari, G., and Szabo, A. (1992) *J. Am. Chem. Soc. 114*, 4546−4559; 4559−4570.
37. Mandel, A. M., Akke, M., and Palmer, A. G. (1994) *J. Mol. Biol. 246*, 144−163.
38. Brüschweiler, R., Liao, X., and Wright, P. E. (1995) *Science 268*, 886−889.
39. Tjandra, N., Feller, S. E., Pastor, R. W., and Bax, A. (1995) *J. Am. Chem. Soc. 117*, 12562−12566.
40. Zheng, Z., Czaplicki, J., and Jardetzky, O. (1995) *Biochemistry 34*, 5212−5223.
41. Schurr, J. M., Babcock, H. P., and Fujimoto, B. S. (1994) *J. Magn. Reson., Ser. B 105*, 211−224.
42. Woessner, D. E. (1962) *J. Chem. Phys. 37*, 647−654.
43. Silver, E. T., Gwozd, T. J., Ptak, C., Goebl, M., and Ellison, M. I. (1992) *EMBO J. 11*, 3091−3098.
44. Chen, P., Johnson, P., Sommer, T., Jentsch, S., and Hochstrasser, M. (1993) *Cell 74*, 357−369.
45. Ptak, C., Prendergast, J. A., Hodgins, R., Kay, C. M., Chau, V., and Ellison, M. J. (1994) *J. Biol. Chem. 269*, 26539−26545.
46. Gwozd, C. S., Arnason, T. G., Cook, W. J., Chau, V., and Ellison, M. J. (1995) *Biochemistry 34*, 6296−6302.
47. Wennerström, H. (1972) *Mol. Phys. 24*, 69−80.
48. Prendergast, J. A., Ptak, C., Arnason, T. G., and Ellison, M. J. (1993) *J. Biol. Chem. 270*, 9347−9352.

BI981840H